THE JOURNAL OF PHYSICAL CHEMISTRY A

Article

pubs.acs.org/JPCA

Accessing Multiple Conical Intersections in the 3s and 3p$_x$ Photodissociation of the Hydroxymethyl Radical

Chirantha P. Rodrigo, Chuanchuan Zhou, and Hanna Reisler*

Department of Chemistry, University of Southern California, Los Angeles, California 90089-0482, United States

Supporting Information

ABSTRACT: The photodissociation dynamics of the hydroxymethyl radical (CH_2OH, CH_2OD, and CD_2OD) following excitation to the 3s and 3p$_x$ Rydberg states is studied using time-sliced velocity map imaging of hydrogen photofragments. Dissociation takes place on the ground potential energy surface reached via conical intersections from the excited states, and formaldehyde and hydrxymethylene are identified as reaction products. The major product, formaldehyde, has a bimodal internal energy distribution. The largest fraction has high kinetic energy (KE), modest rotational excitation, and vibrational excitation mainly in the CO stretch and the $CH(D)_2$ deformations modes (scissors, wag, and rock). The minor fraction has lower KEs and a higher rovibrational excitation that is unresolved. A bimodal internal energy distribution in the formaldehyde fragment has been predicted by Yarkony [*J. Chem. Phys.* **2005**, *122*, 084316] for a conical intersection along the O−H bond coordinate. The hydroxymethylene product state distributions depend strongly on the nature of the excited state. In dissociation via the 3s state, the hydroxymethylene products have broad rovibrational state distributions and are produced at low yield. As suggested by Yarkony, they may be produced in the same dissociation events that give rise to low KE formaldehyde. In these events, the bound region of the PES is sampled following the conical intersection along O−H(D). The hydroxymethylene yield is low near its threshold and increases slowly with excitation energy to the 3s state, but its internal energy distribution remains broad and the contributions of the cis- and trans-isomers cannot be resolved. The mechanism changes markedly when exciting to the 3p$_x$ state. The hydroxymethylene products have less rotational excitation and show separate contributions of cis- and trans-isomers. The trans-isomer is found to be a minor product relative to the higher-energy cis-isomer, as predicted by Yarkony for conical intersections along the C−H coordinate. It appears that the efficiency of dissociation via conical intersections along the O−H and C−H coordinates depends on the initial excited state. While the O−H conical intersection seam (vertical cone) provides an efficient route to the ground state following excitation via the 3s or the 3p$_x$ Rydberg states, conical intersections along the C−H bond coordinate (tilted cone) are sampled more efficiently via 3p$_x$ excitation and proceed through different dynamics. The energy separations between formaldehyde and hydroxymethylene and between the cis- and trans-isomers of hydroxymethylene are determined experimentally for all the investigated isotopologs and are in good agreement with theory.

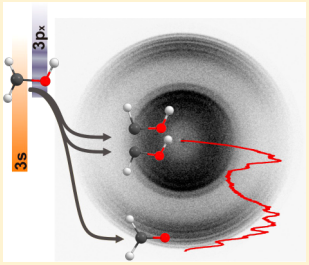

I. INTRODUCTION

The hydroxymethyl radical has been implicated in atmospheric, astrochemical, and combustion processes. For example, CH_2OH is a significant product in the reaction of $O(^1D)$ with methane,[1,2] while reactions of Cl and H atoms with methanol yield predominantly CH_2OH.[3,4] In addition, the hydroxymethyl radical and its isomer, the methoxy radical, are implicated in reactions such as O + CH_3 and O_2 + CH_3OH.[5−8] Recently, it has been suggested that hydroxymethyl radicals might be present in the interstellar medium under conditions where methanol is ubiquitous.[9−12] It is no wonder, therefore, that much research, theoretical and experimental, has been devoted to this radical.[13−38] While the ground state of CH_2OH has been well characterized[14,18,26−29,33,36,37] and its predissociation and isomerization pathways investigated recently in detail,[27,32,34] much less information is available on its excited states photophysics and photodissociation dynamics.

Previously it has been established that the onset of electronic absorption in CH_2OH is at ∼26 000 cm^{-1} and the radical continues to absorb at least up to 45 000 cm^{-1}.[20,22,23] Three Rydberg states contribute to the absorption.[15,16,22,25,26,35] (1) Absorption to the 3s($1^2A'$) state has an onset at 25 970 cm^{-1} and extends all the way up to the highest wavelengths investigated so far. This absorption system is structureless.[22] (2) The origin band of the absorption to the 3p$_x$($2^2A'$) state lies at ∼35 000 cm^{-1} and has a width of >100 cm^{-1} due to lifetime broadening. This absorption system, which lies above a structureless background of continuing 3s absorption, exhibits a progression in the CO stretch.[22] (3) Absorption to the 3p$_z$($2^2A''$) state has a clear vibronic band structure with linewidths ∼10 cm^{-1} and an origin band at 41 050 cm^{-1}. It shows a progression in the CO stretch and has other assigned vibronic bands.[22,26,38] All the states are short-lived (<0.5 ps), and H atoms are the main photodissociation products.[20−23]

Special Issue: Curt Wittig Festschrift

Received: May 7, 2013
Revised: July 12, 2013

   dx.doi.org/10.1021/jp404552g | *J. Phys. Chem. A* XXXX, XXX, XXX−XXX

Electronic structure calculations are in agreement with these assignments.[15,16,25,35]

The lowest Rydberg states are obtained by promoting an electron from the half-occupied π^*_{CO} antibonding molecular orbital to a Rydberg orbital localized on carbon.[15,16,25,26,35] This results in an increased CO double bond character in the Rydberg states and a concomitant large change in the CO bond length.[26] The ground state is nonplanar and rigorously should be treated with the G4 group in the permutation-inversion model. However, as shown before, the electronic wave function complies with C_s symmetry, as do the Rydberg states, and therefore, the vibrationless electronic states are symmetry labeled as A″ and A′.[26]

Previous studies have shown that the Rydberg states of CH_2OH are coupled to the ground state, leading to O−H and C−H bond breaking and generating formaldehyde and hydroxymethylene dissociation products.[20−23,25,35] The lowest channels have the following dissociation energies:

$$CH_2OH \rightarrow CH_2O(\tilde{X}^1A_1) + H;$$
$$D_0 = 10160 \pm 70\ cm^{-1}\ (1.26 \pm 0.01\ eV) \quad (I)$$

$$CH_2OH \rightarrow trans\text{-}CHOH(\tilde{X}^1A') + H;$$
$$D_0 = 28420 \pm 70\ cm^{-1}\ (3.52 \pm 0.01\ eV) \quad (II)$$

$$CH_2OH \rightarrow cis\text{-}CHOH(\tilde{X}^1A') + H;$$
$$D_0 = 29970 \pm 70\ cm^{-1}\ (3.52 \pm 0.01\ eV) \quad (III)$$

D_0 for channel I was determined by Ryazanov and Reisler[32] and those for channels II and III in the present work. Slightly different values are obtained for CH_2OD. The two dissociation channels are correlated with ground-state CH_2OH, which is reached via conical intersections from the $3s(^2A')$ and $3p_x(^2A')$ Rydberg states that lie >2 eV above the H + CH_2O asymptote.[25,35]

In previous work with CH_2OD, we recorded H and D photofragments yield spectra following excitation to the Rydberg states.[22] At 26 000−30 000 cm^{-1} only O−D bond-breaking was observed, whereas at photolysis energies >30 500 cm^{-1} both D and H products were detected. The H/D ratio increased fairly monotonically with photolysis energy.

The kinetic energy distributions (KEDs) of D fragments from CH_2OD (O−D bond fission) determined by core-sampling time-of-flight (TOF) spectroscopy have revealed that much of the available energy is channeled into translation.[20,21] The recoil anisotropy parameter, β, was close to its asymptotic value of −1.0, indicating fast dissociation following a perpendicular transition. However, the rovibrational levels in the formaldehyde cofragment could not be resolved using TOF detection. The KEDs determined by monitoring H photofragments from C−H bond fission were very different.[21] They exhibited lower maximum kinetic energies (KEs), as required by the thermochemistry of channels II and III, and the distributions were broad and nearly isotropic, encompassing all the allowed kinetic energies.

Hoffman and Yarkony[25,35] carried out conical intersection calculations that were pivotal to interpretations. They pinpointed pathways for radiationless decay and identified efficient crossing seams between 3s and the ground state and between $3p_x$ and 3s that lead to O−H and C−H bond breaking. For example, a low-energy crossing seam between 3s and the ground state was identified at an O−H distance R(OH) = 1.48 Å, extended by about ∼0.5 Å from the equilibrium O−H distance in the ground state. The vertical cone for this intersection promotes coupling to the ground state. Consequenty, Yarkony predicted that most of the CH_2OH radicals would dissociate directly to CH_2O + H on the repulsive part of the potential energy surface (PES) along R(O−H) on the ground state.[35] Our observations were consistent with this analysis.[20,21]

In a later paper,[35] Yarkony re-examined the conical intersection seams using higher-level theory, and analyzed gradients on the ground state following conical intersections with 3s by looking at the so-called g and h vectors and the associated nuclear motions on the ground state PES. This allowed him to make several predictions to which we will come back later. He proposed, for example, that in addition to the motions that result in O−H bond breaking on the repulsive part of the PES, gradients on the ground state can also lead to *reduction* in R(OH), propelling a fraction of the radicals toward the minimum energy geometry on the ground state. This pathway should lead to a more statistical outcome in the dissociation and provide routes on the ground PES to both C−H and O−D bond breaking channels in CH_2OD photodissociation. In this mechanism, HCOD would form first in its lowest energy trans-isomer and then the cis-isomer would be populated in turn.

However, Yarkony showed that the conical intersection seam between 3s and the ground state that leads to direct C−H bond fission (tilted cone) takes place at large R(C−H), and can be reached only at energies above the H + HCOD asysmptote over a small barrier. He predicted that this conical intersection would lead predominanty to formation of the higher-energy *cis*-HCOD and that this seam would become more accessible at higher excitation energies. According to Hoffman and Yarkony,[25] when the radical is excited to the $3p_x$ state, it would first couple to 3s via a conical intersection seam (tilted cone), and subsequently to the ground state via the conical intersections described above, finally leading to O−D and C−H bond breaking. This analysis underscores the strong effects of gradients near the conical intersections on nuclear motions.

Recently, we developed an improved sliced velocity map imaging (SVMI) experimental arrangement optimized for detecting hydrogen fragments,[39] and used it to study the overtone-induced dissociation and isomerization pathways on the ground state of CH_2OH and CD_2OH.[32] The H and D fragment KEDs were structured, indicating which vibrational levels in the formaldehyde cofragment were excited. In the present work, we use the same experimental arrangement to focus on the photodissociation dynamics of isotopologs of the hydroxymethyl radical (CH_2OH, CH_2OD, and CD_2OD) following excitation to the 3s and $3p_x$ Rydberg states. We were inspired to return to these experiments by Yarkony's predictions regarding channels I−III.[35]

An advantage in studying the photodissociation of the hydroxymethyl radical is its continuous absorption from ∼26 000 cm^{-1} onward, which allows interrogation of specific processes at optimal excitation energies.[22,23,31] Figure 1 shows the excited states and product channel energies that are relevant to the present study. We focus mainly on excitation energies near the opening of the hydroxymethylene channel and the region around the origin band of the $3p_x$ state. The use of different isotopologs helps sort among mechanisms, thereby solidifying interpretations.

dx.doi.org/10.1021/jp404552g | J. Phys. Chem. A XXXX, XXX, XXX−XXX

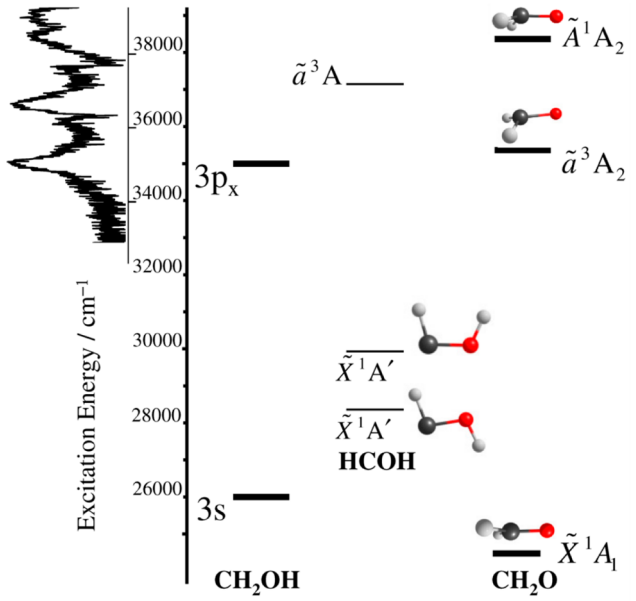

Figure 1. Excited states and fragment channel energies. Superimposed on the left is the structured absorption spectrum in the region of excitation to the 3p$_x$ state (ref 22). Structureless absorption to the 3s state, which starts at ~26 000 cm^{-1}, underlies the 3p$_x$ absorption spectrum as background.

II. EXPERIMENTAL DETAILS

The experimental setup and conditions were similar to those reported previously[32,39,40] and are only described briefly here. A molecular beam of cold hydroxymethyl radicals (rotational temperature = 10−15 K) or their isotopologs is excited to the two lowest Rydberg states by UV laser radiation, and H/D photoproducts are detected by SVMI after excitation to their respective ions (H^+/D^+).

The generation of the CH_2OH radical and its isotopologs in a supersonic expansion and the detection of H/D photofragments have been described previously.[20−22,32] In brief, reactant mixtures of Cl_2 (0.5%; Matheson AirGas, 99.95% purity) and CH_3OH (3%) or its isotopologs CH_3OD and CD_3OD (Aldrich, used without further purification) are prepared in a glass bulb (5.0 L) in He. The final pressure of the mixture is 2.0 atm at room temperature. The gas mixture is introduced into the vacuum chamber via a piezoelectrically driven pulsed valve operating at 10 Hz. Hydroxymethyl radicals are produced by the reaction of methanol with Cl atoms generated by 355 nm photodissociation of Cl_2 inside a quartz tube (length = 7 mm; Ø = 1 mm) attached to the orifice of the nozzle. The 355 nm radiation (~13 mJ; third harmonic of Quanta-Ray GCR-11 Nd:YAG laser, 10 Hz) is focused with a cylindrical lens as described before.[22,32] The molecular beam passes through a skimmer (Beam Dynamics, Ø = 1 mm) before entering the detection region of the vacuum chamber.

In the detection region, the skimmed molecular beam is intersected at right angles by two counter-propagating laser beams. Mildly focused UV laser radiation at 364−273 nm (0.8−2.5 mJ/pulse, lens focal length (f.l.) = 30 cm) excites the radical to selected energies of the 3s and 3p$_x$ Rydberg states. The UV pump radiation is obtained from a Nd:YAG laser pumped dye laser system (Continuum, PL8000/ND6000 10 Hz;). H(D) fragments are detected by 1 + 1′ resonance enhanced multiphoton ionization (REMPI). Laser radiation at 121.59 and 364.8 nm excites and ionizes H atoms via the Lyman-α transition (the corresponding wavelengths for D detection are 121.56 and 364.7 nm). The VUV radiation is generated by tripling ~365 nm radiation in a frequency tripling cell with a mixture of Kr and Ar by focusing 2−3 mJ of the ~365 nm doubled output of a Nd:YAG laser pumped dye laser system (Continuum, NY-81C/ND6000; LDS 722 dye, Inrad Autotracker-II doubler with KDP crystal, lens f.l. = 20 cm). The residual ~365 nm radiation that passes through the cell ionizes the excited H(D) fragments. The probe laser is delayed by ~2 ns with respect to the pump laser, and its wavelength is tuned across the Doppler profile of the H(D) fragments while recording velocity map images.

Two different types of experiments were performed: (1) in probe-only experiments, residual 365 nm radiation from the probe laser acts as the pump laser; (2) in pump−probe experiments, a separate UV pump laser is used to excite the radical to selected excitation energies and H(D) atoms are probed as described above. In these experiments, the probe laser power is turned down to minimize background signal generated by residual ~365 nm. This background is subtracted from the images before processing the data.

The SVMI arrangement and operation procedures have been described in detail before.[32,39,40] The time spread of the ion cloud is stretched to ≥50 ns by optimizing the SVMI operating conditions with the aid of ion trajectory simulations.[39,40] A thin time slice of the ion cloud (<10% of the total) is taken from the center and imaged onto a position sensitive detector by fast gating the MCP gain. This is accomplished with a homemade high-voltage pulser that generates ≤5 ns pulses.[39,40] The center slice is located by taking several short acquisitions of images around the center of the ion cloud and comparing them for two features that indicate the center: (i) the sharpness of the ring structures in the image and (ii) the largest image size. This procedure determines the optimal time delay between the pump laser firing and the gating pulse.

Ion spot locations (hit events) on the detector are stored in a computer as Cartesian coordinates and later transformed to polar coordinates. Radial distributions were obtained summing all events in full 360° at each radius R. All images are rectified for slight imperfections in the radial distributions as described elsewhere.[40] The speed (velocity) distributions of H(D) fragments are derived from the radial distribution of ions using the appropriate calibration factors based on dissociation events of known recoil energy.[39] Center-of-mass kinetic energy distributions (KEDs) are obtained by using momentum conservation and the corresponding Jacobian, and recoil anisotropy parameters are determined from the angular distributions at each R in the usual way.[40]

For CD_2OD, structure optimization and vibrational frequency calculations were performed at the MP2/6-311+G-(2d,p) level of theory. It has been shown before by Blowers and Masel[41] that for CH_nOH_m (n and m are integers) type molecules the above level of calculations gives good agreement with experiment after using a scaling factor of 0.96. Calculations were carried out using the Q-CHEM computational package.[42]

III. RESULTS

H and D photofragment images were recorded at several excitation energies that access the 3s and 3p$_x$ Rybderg states (Figure 1). In particular, we concentrated on the following excitations: (i) below the energetic opening of the hydroxymethylene channels; (ii) near the thresholds of *cis*- and *trans*-hydroxymethylene; and (iii) near and at the band origin of the

dx.doi.org/10.1021/jp404552g | J. Phys. Chem. A XXXX, XXX, XXX−XXX

transition to the $3p_x$ state. By using different isotopologs, identifying background contributions and fitting fragment state distributions were facilitated.

Before processing the images contributions from background signals had to be removed. Signals from probe laser dissociation were removed by recording probe-only images, while maintaining the same experimental conditions except for blocking the pump laser, and subtracting them from the pump−probe images. Background signals due to isotopic contamination were removed as described by Feng et al.[21] H fragment images from CH_2OD included small contributions from contaminant CH_2OH. This background was estimated and removed from CH_2OD images by recording images of neat CH_2OH and scaling them to match the intensity of high KE H fragment signals generated by O−H bond breaking in CH_2OH before subtraction. Images acquired upon excitation to the $3p_x$ state include small contributions from underlying 3s dissociation. Because the KEDs associated with hydroxymethylene products are very different for 3s and $3p_x$ dissociation (see below), it was possible to estimate these contributions, and the signals associated with 3s dissociation were subtracted from the images acquired in the $3p_x$ absorption region before attempting to fit the KEDs. This subtraction procedure was only applied for the purpose of fitting and assigning structures in the KEDs of hydroxymethylene.

In order to fit the KEDs with vibrational levels of the products, we used the PGOPHER software program,[43] which allowed also determination of rotational temperatures. First, a stick spectrum of the energetically allowed vibrational levels of each product was generated, and a rotational temperature was selected for best fit. We assumed the same rotational constants for all vibrational states regardless of the level of excitation. Tables 1 and 2 list the rotational constants and fundamental

Table 1. Vibrational Frequencies and Rotational Constants of Formaldehyde in the Ground State (in cm^{-1})[a]

rotational constant		CH_2O	CD_2O
A		9.408	4.726
B		1.296	1.077
C		1.135	0.874
vibrational description (symmetry)			
sym. C−H stretch	ν_6 (a_1)	2783	2056
C−O stretch	ν_2 (a_1)	1746	1702
CH_2 scissors	ν_3 (a_1)	1500	1106
CH_2 wag	ν_4 (b_1)	1167	938
antisym. C−H stretch	ν_5 (b_2)	2843	2160
CH_2 rock	ν_6 (b_2)	1249	989

[a]From ref 44.

vibrational frequencies used for the formaldehyde and hydroxycarbene isotopologs. Vibrational frequencies of fundamentals, overtones and combinations bands were taken from the literature when available.[44,45] Other energy levels were generated by combinations of fundamental frequencies obtained either from calculations[46−48] or from experimental measurements.[48]

Contour fittings were begun with the vibrationless peak by varying its KE origin and rotational temperature to match the experimental profile. Linewidths (Gaussian shapes) were added to each rotational line to simulate the experimental resolution.[40] Special attention was paid to fitting well the rise and tailing-off of the band contours by varying both the temperature and linewidth. The optimized rotational temperatures and widths were used to fit the remaining vibrational bands for each fragment, leaving only the relative populations (intensities) as variables. Two different rotational temperatures were used to simulate *cis*- and *trans*-HCOH products as they showed different degrees of tailing-offs in their experimental distributions. A least-squares fitting algorithm was used to fit the part of the KED correlated with the formaldehyde cofragment, which had partially resolved structures. Other parts of the KEDs were fit by manual adjustments of populations while seeking optimal visual fits.

The best signal-to-noise ratio in the KEDs was obtained for H/D images recorded with ∼365 nm excitation. This residual radiation from the tripling cell (used to ionize the excited H/D fragments) also causes dissociation of the hydroxymethyl radical via channel I. The excitation energy of ∼27 400 cm^{-1} is insufficient for reactions II and III. In pump−probe experiments, the small signal from the probe laser is subtracted before analysis as described above, but with increased intensity of the 365 nm radiation, significant H/D fragment signals are obtained without firing the pump laser. Figure 2 shows images obtained by detecting H/D fragments from CH_2OH, CH_2OD, and CD_2OD, and the corresponding kinetic energy release (KER) plots. In comparing the KEDs obtained from H/D images of CH_2OH and CH_2OD, we observe larger signals at very low KEs from the former. The excess signal that extends down to zero KE corresponds to a small background of unknown origin. In CH_2OD experiments, the H and D contributions are separated, demonstrating that the small contaminant signal at low KE is associated only with H atoms but not D fragments (see Figures S1 and S2 in Supporting Information for examples of this background). This signal must be associated with an unknown background contamination because at this energy the C−H bond cannot be broken. A similar low KE background exists in D images from CD_2OD as seen in Figure 2c. Since this part of the KED is structureless and we only fit the structured, high KED component in these images, this background does not cause interference.

The structured components in the three KEDs shown in Figure 2 can be fit by using the known vibrational levels of formaldehyde listed in Table 1.[44] Attempts to fit the KEDs by assuming only CO stretch (ν_2) excitation or any other single vibrational mode failed to give good fits (see Figure S3 in the Supporting Information). We found that the CH(D) stretch modes do not contribute, but inclusion of both the CO stretch and $CH(D)_2$ deformation modes (rock, wag, and/or scissors) was needed. As these modes are quite close in energy (see Table 1) it was difficult to determine which one is dominant. Figure 2 shows the best fit for each isotopolog obtained by using the CO stretch ν_2 and the CH_2 scissors ν_3 modes. The vibrational levels used in the fits are marked with stick spectra, in which the position of the line indicates the origin of the rotationless vibrational level, and its length is proportional to the integrated population of the level. The relative populations of the vibrational levels that give rise to the displayed fits are listed in the Supporting Information (Figures S4−S7 and Tables S1−S3).

For CH_2OH and CH_2OD, the structures correlated with CH_2O are fit satisfactorily by assuming the participation of the CO stretch ν_2 and the CH_2 scissors mode ν_3. However, these fits are not unique, and fits using the other CH_2 deformation modes in addition to the CO stretch (while varying somewhat

dx.doi.org/10.1021/jp404552g | J. Phys. Chem. A XXXX, XXX, XXX−XXX

Table 2. Vibrational Frequencies and Rotational Constants of Hydroxycarbene isotopologs (in cm^{-1})

		HCOH[a]		HCOD[a]		DCOD[a]	
rotational constant		*trans*	*cis*	*trans*	*cis*	*trans*	*cis*
A		9.701	9.346	7.393	6.901	5.754	5.006
B		1.222	1.217	1.139	1.142	1.031	1.057
C		1.085	1.077	0.987	0.980	0.875	0.873
vibrational description	**(symmetry)**	***trans*-HCOH[b]**	***cis*-HCOH[c]**	***trans*-HCOD[b]**	***cis*-HCOD[c]**	***trans*-DCOD[d]**	***cis*-DCOD[d]**
o.p. twist	ν_6 (a'')	1058.9 (*1048.5*)	978	907.1 (*901.6*)	847	790	761
i.p. bend	ν_5 (a')	1183.5 (*1183.2*)	1189	928.7 (*923.1*)	921	862	857
i.p. bend	ν_3 (a')	1475.1 (*1465.5*)	1442	1420.8 (*1414.7*)	1414	1280	1278
C−O stretch	ν_4 (a')	1300.5 (*1297.1*)	1299	1294.1 (*1290.8*)	1288	1116	1120
C−H stretch	ν_2 (a')	2706.5, 2785.5 (*2703.3, 2776.2*)	2552	2682.8 (*2675.9*)	2516	2086	2023
O−H stretch	ν_1 (a')	3561.6, 3520.8, 3516 (*3500.6*)	3397	2566.4, 2626.8 (*2588.1*)	2584	2623	2547

[a]Rotational constants generated from molecular geometries given in ref 48. [b]From ref 48. VCI frequencies. Experimental values are given in parentheses. [c]From ref 47. VCI frequencies. [d]This work. Scaled frequencies (0.96 scaling factor).

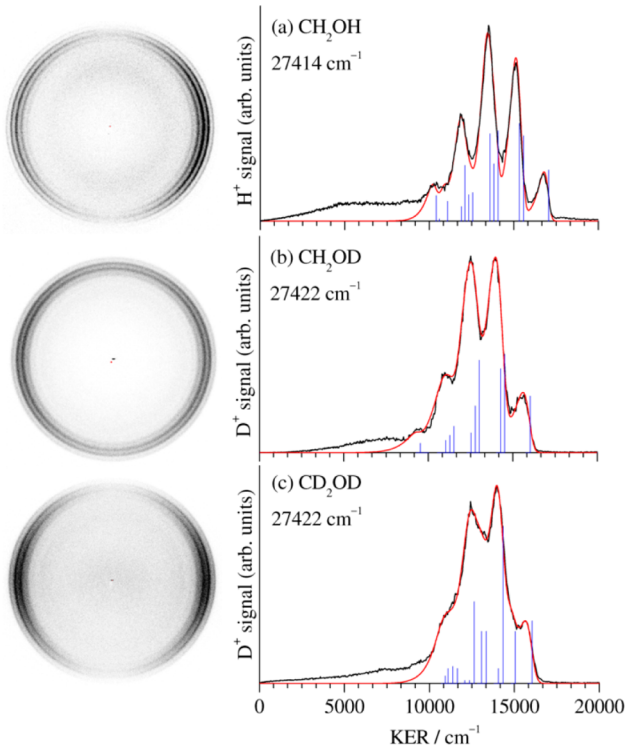

Figure 2. H/D photofragment images and the corresponding kinetic energy release (KER) plots (black curves) obtained in probe-laser only dissociation of (a) CH_2OH, (b) CH_2OD, and (c) CD_2OD. The stick spectra that give the best fits to the KEDs (red curves) correspond to vibrational levels of formaldehyde, with the length of each line proportional to the integrated relative population of each level. The excited vibrational levels include the CO stretch ν_2 and combination bands with the scissors mode ν_3. See the text for details.

the rotational temperature) are satisfactory as well (see Figure S5 and Table S1 in the Supporting Information). In addition, we are mindful of the fact that the rotational energy distributions may not be simulated well by a temperature and that Gaussian-shaped rotational distributions are often generated in dissociation on repulsive surfaces. Therefore, temperature is considered here only as a number of merit for the extent of rotational excitation. Nevertheless, to achieve the best fits, both CO stretch excitation and the CH_2 deformation modes are required (overtones and combination bands). The rotational temperature returned by the fits is 450−550 K, corresponding to 312−382 cm^{-1} of fragment rotational energy.

Because the frequencies of the deformation modes of CH_2OH and CH_2OD are quite similar to the CO stretch, the peaks in the KEDs consist of clumps of close-lying vibrational levels. This results in fairly well resolved structures in the KEDs despite the inclusion of numerous vibrational levels in the fits. The situation is different for CD_2OD. Here, the frequencies of the CO stretch (1702 cm^{-1}) and the CD_2 deformation modes (989, 938, and 1106 cm^{-1}) are disparate, and thus, the overtones and combination bands span almost the entire KE range. Indeed, in this case, the structures in the KEDs are less resolved, as seen in Figure 2c. The best fit for CD_2OD is obtained by assuming the participation of the CO stretch and the CH_2 scissors (ν_3). The fits show that some of the populations of the close-lying levels are quite correlated, and therefore, we show stick spectra rather than report accurate population distributions.

The maximum KER in each curve corresponds to the dissociation energy of channel I. The value obtained for CH_2OH, 10340 ± 140 cm^{-1}, agrees within experimental error with the previous result of 10160 ± 70 cm^{-1}.[32] The corresponding values for CH_2OD and CD_2OD, 11402 ± 140 and 11440 ± 140 cm^{-1}, respectively, are listed in Table 3.

From the angular distributions, we determine the recoil anisotropy parameters β for the structured components at high KE to be ∼−0.7, in agreement with previous results.[20−22] The lower energy, structureless components of the KEDs have values much closer to zero or slightly negative. We will return to the anisotropy issue later.

We have recorded images at other excitation energies that access the 3s state, and the general appearance of the structured component of the KEDs does not change, as seen in Figures 3 and 4. The main change is that the signal level increases at

dx.doi.org/10.1021/jp404552g | J. Phys. Chem. A XXXX, XXX, XXX−XXX

Table 3. Dissociation Energies (D_0) Determined from KEDs of H(D) Photofragments and Energy Separations between *cis*- and *trans*-HCOH isotopologs; Energy Calibration and Fitting Errors Are Included in the Confidence Error Bars

reaction	D_0 (cm^{-1})	$E_{cis-trans}$ (cm^{-1})
$CH_2OD \rightarrow H_2CO + H$	10340 ± 140	
$CH_2OH \rightarrow$ *trans*-HCOH + H	28424 ± 70	
$CH_2OH \rightarrow$ *cis*-HCOH + H	29974 ± 70	1550 ± 40
$CH_2OD \rightarrow H_2CO + D$	11402 ± 140	
$CH_2OD \rightarrow$ *trans*-HCOD + H	28385 ± 70	
$CH_2OD \rightarrow$ *cis*-HCOD + H	29945 ± 70	1560 ± 40
$CD_2OD \rightarrow D_2CO + D$	11440 ± 140	
$CD_2OD \rightarrow$ *trans*-DCOD + D	28955 ± 70	
$CD_2OD \rightarrow$ *cis*-DCOD + D	30590 ± 70	1635 ± 40

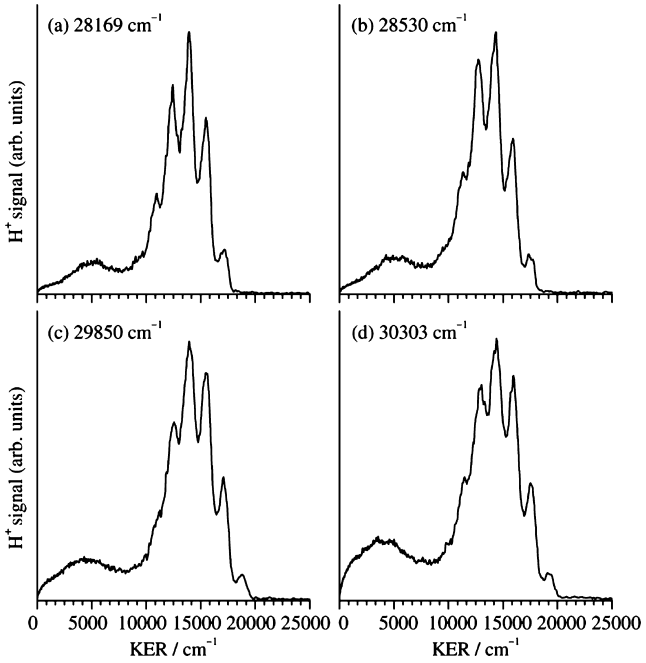

Figure 3. H photofragment KEDs obtained in 3s dissociation of CH_2OH at the indicated energies. The background from probe-laser only dissociation is subtracted.

higher photolysis energies as the maximum in the 3s absorption cross-section is approached, and the internal excitation in the formaldehyde fragment increases somewhat.

The low KE region in the KEDs changes qualitatively when exciting in the peak of the origin band of the transition to $3p_x$. Figures 4 and 5 compare H/D images recorded for excitation of CH_2OH and CH_2OD just below the origin band of the $3p_x$ transition band and at its peak. The same qualitative shapes of the KEDs are observed for all three isotopologs. At these photolysis energies, the hydroxymethylene channels II and III are open, with 20−30% of the products arising from breaking the C−H(D) bond.[20−22] We can now examine the photodissociation via these channels with better KE resolution.

Just prior to the opening of the $3p_x$ transition, the KEDs of CH_2OH and CD_2OD are typical of those for 3s excitation. They include a structured, high KE component as before, and also a prominent low KE component that is unstructured and is composed in part of H/D from O−H(D) bond breaking processes (similar to the KEDs observed at energies below the energetic opening of channels II and III), and a component

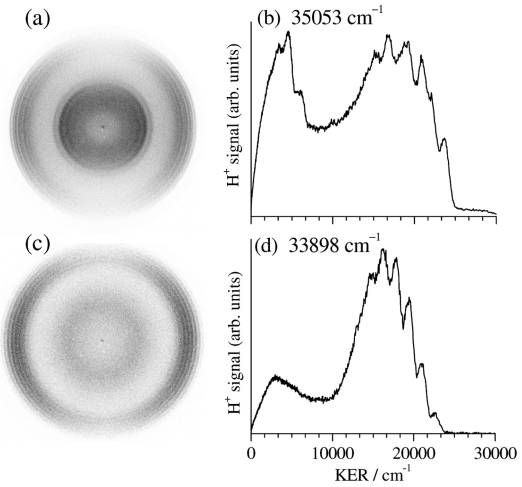

Figure 4. H photofragment images and KEDs obtained in CH_2OH dissociation: (a,b) at the peak of the origin band of $3p_x$ absorption (35 053 cm^{-1}) and (c,d) at 33 898 cm^{-1} (3s absorption), just below the $3p_x$ band origin. Note the difference in structure in the low KE component correlated with HCOH production and the change in relative integrated intensities of the low and high KE components.

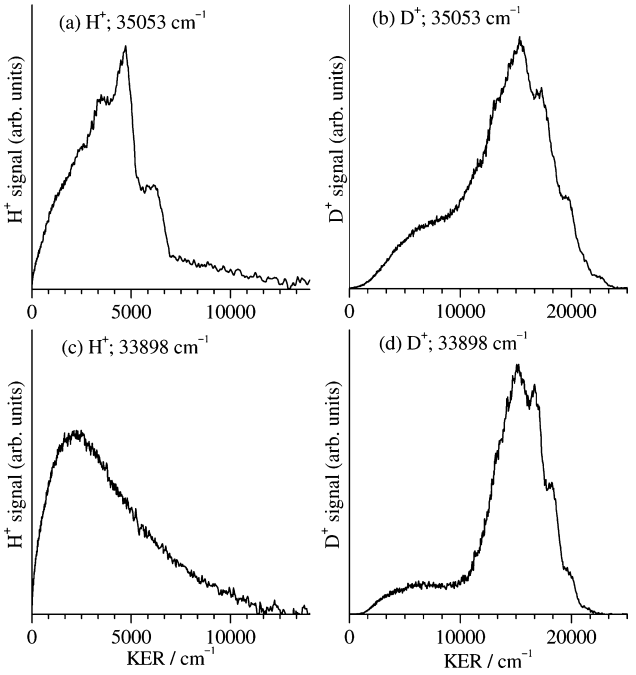

Figure 5. H and D photofragment KEDs obtained in CH_2OD dissociation: (a,b) at the peak of the origin band of $3p_x$ absorption (35 053 cm^{-1}) and (c,d) at 33 898 cm^{-1} (3s absorption), just below the $3p_x$ band origin. Signals due to a small amount of CH_2OH in the sample have been subtracted from the H-fragment KER plots as explained in the text. Also, the small signal in (a) that extends to high KEDs beyond ~6800 cm^{-1} derives from an unknown contamination. This signal cannot be separated in panel c because of the lack of structure in the low KE part. The signal height in each plot is in arbitrary units and does not reflect the relative population of CH_2O and HCOD.

correlated with breaking the C−H(D) bond that extends down to zero KER .[20−22] These two components are distinguished in CH_2OD, as shown in Figure 5c,d. The H-fragment KER from C−H bond breaking indeed extends to zero KER.

dx.doi.org/10.1021/jp404552g | J. Phys. Chem. A XXXX, XXX, XXX−XXX

The shapes of the KEDs in the low KE region change abruptly when exciting to the $3p_x$ state. In all three isotopologs, the low KE component exhibits structures with sharp rises that coincide with vibrations of hydroxymethylene (see below). In addition, Figure 4 shows that the relative population of the low KE component increases relative to the population of the higher KE component when compared to the corresponding population ratios obtained in 3s excitation just below the origin of the $3p_x$ transition. Figure 5a,b, which shows H and D signals from CH_2OD, distinguishes again between the O−D and C−H bond breaking channels. Inspection of the H-fragment KEDs (Figure 5a,c) shows that the major change in going from 3s to $3p_x$ excitation is in the internal energy distribution in the HCOD radical, in particular the reduction in rotational temperature. The appearance of distinct structures with sharp rises in Figure 5a allows us to distinguish between signal correlated with the HCOD fragment, which appears with a maximum KE of 6670 cm^{-1}, and the small, structureless background that extends from near zero KE to >12 000 cm^{-1}, and is attributed to the small contamination discussed above.

Previously, H signals from CH_2OD dissociation were reported to have an onset at ∼30 500 cm^{-1}, where the H signal was only <0.05 of the D signal.[22] The H/D ratio increased with excitation energy, reaching ∼30% at the origin band of the transition to $3p_x$. With the better sensitivity and KE resolution afforded with the new experimental arrangement, we reexamined the C−H bond breaking. We find that near the threshold of channel II the contaminant H signal obscures the very small signal correlated with *trans*-HCOH, and the threshold for this channel cannot be identified. As shown in Figure 4 for CH_2OH, the low KE signal, which is present at energies below the opening of the channel II, increases only gradually with excitation energy when this channel is energetically open, but no structure is observed. Recording H fragments from CH_2OD does not improve the situation, and thus these measurements do not provide additional information regarding the H/D ratios compared to previous results, and only confirm that at these excitation energies C−H bond breaking is inefficient.

Much more information can be derived from the KEDs obtained following excitation to the $3p_x$ state, in particular those correlated with hydroxymethylene. To this end, we zoom on the low KE region of H/D fragments from the three isotopologs, and the results are shown in Figure 6. In order to assign the structures in the KEDs, background signals associated with isotopic contamination and 3s dissociation are removed, as described above. The highest KE peak in the H fragment KEDs from CH_2OH and CH_2OD appears at an energy corresponding to the ground vibrational level of the *trans*-hydroxymehtylene;[48] it exhibits a sharp rise and a decay that can be simulated with a rotational temperature of ∼1200 K. The derived dissociation energies leading to *trans*-hydroxymethyelene for the three isotopologs are summarized in Table 3.

The second highest-energy peak in the KEDs is the most prominent one, and it also has a fairly sharp rise. In order to fit this peak to a vibrational level of one of the isomers, we use the calculated and/or experimental vibrational energies of *trans*- and *cis*-HCOH(D) summarized in Table 2.[47,48] The trans-vibration closest in energy to this peak is ν_3 (in-plane bend) at 1466 and 1415 cm^{-1} for HCOH and HCOD, respectively, values that are close to the calculated cis−trans energy separation of 1550−1620 cm^{-1}.[46−48] Thus, it is quite challenging to distinguish between these two contributions, and we have relied on the consistency of the fittings of several KEDs for the three isotopologs. We obtain good fits for the first two peaks for all the isotopologs when we assume that the second peak is the ground state of the cis-isomer, and let its rotational temperature vary to achieve the best fit. The fits are consistently inferior when we follow the same procedure but assume that this peak corresponds to ν_3 of *trans*-HCOH(D) (see Figure S8 in Supporting Information). Conversely, when we carry out a free fit of these two peaks, the energy separation that is returned by the fits, 1550−1600 cm^{-1}, is closer to the calculated cis−trans separation than to the ν_3 energies of HCOH(D). We note that the cis-isomer has never been isolated experimentally, and we must rely on theoretical calculations of the vibrational energies and the cis−trans energy separation. Our interpretation is strengthened by experiments with CD_2OD. As shown in Table 2, there is no vibrational mode of DCOD whose frequency is close to the cis−trans energy separation of ∼1600 cm^{-1}. Fitting the two peaks in the KED shown in Figure 6c gives an energy

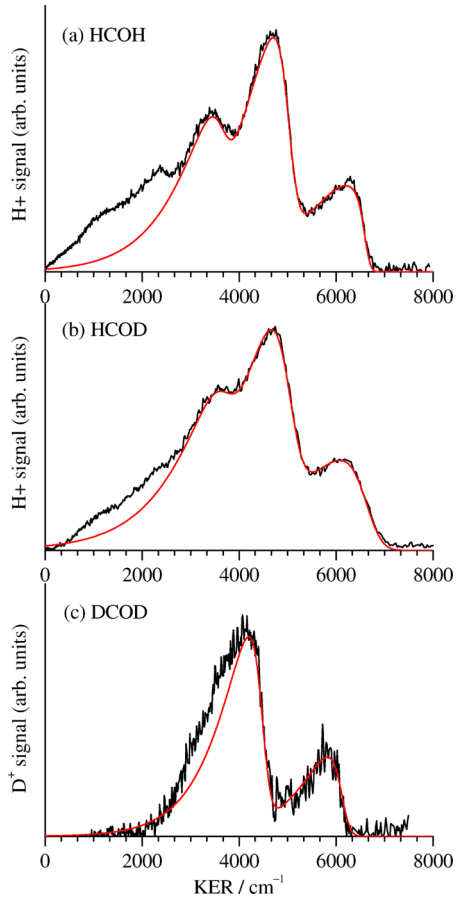

Figure 6. KER plots (black curves) obtained from images in which the low KE region was expanded to fill the detector. Excitation to the origin band of the $3p_x$ transition (35 053 cm^{-1}) was used in (a) CH_2OH, (b) CH_2OD, and (c) CD_2OD. Background signals were subtracted as explained in the text. The red curves show best fits using vibrational levels of *trans*- and *cis*-hydroxymethylene. The two highest KE peaks are assigned as the ground states of the trans- and cis-isomers and are separated by 1550, 1560, and 1635 cm^{-1} in (a), (b), and (c), respectively. The next peak in parts a and b is fit by assuming excitation to the CO stretch ν_4 of HCOH(D).

dx.doi.org/10.1021/jp404552g | J. Phys. Chem. A XXXX, XXX, XXX−XXX

separation of ~1630 cm^{-1}, confirming that the second peak is indeed correlated with *cis*-DCOD.

Assigning the second peak in the HCOH(D) KEDs as the ground state of *cis*-HCOH(D) leads to assignment of the third peak as the CO stretch (ν_4; ~1300 cm^{-1}) of the cis-isomer. Results obtained at other excitation energies coinciding with vibronic bands of the $3p_x$ transition (see Figure S9, Supporting Information, for examples) confirm this interpretation. We have not tried to assign the rest of the structures in the KEDs because of the large number of possible levels and the high rotational excitation that masks vibrational structure. We do note, however, that with excitation at higher energies, e.g., coinciding with excitation to the CO stretch level of $3p_x$,[22] the intensity of the peak assigned to the trans-isomer decreases relative to the peak that is best fit as the ground state of the *cis* isomer (see Figure S9 in Supporting Information).

IV. DISCUSSION

Previous work on CH_2OD has shown that in addition to O−H bond breaking, C−H fission becomes possible starting at energy ~30 540 ± 1000 cm^{-1}, and that the H/D ratio increases fairly monotonically up to at least 42 000 cm^{-1}.[22] The observed 4540 cm^{-1} energy difference between the onsets of D and H formation indicates that two separate processes contribute to the formation of CH_2O and HCOD and that isomerization to methoxy is not important. The two channels have different angular distributions as well, with β parameters of ~−0.7 and 0 to −0.4 for the O−D and C−H channels, respectively.[22] With better KE resolution, we are now able to take a closer look at the photodissociation dynamics by varying the excitation energy and using several isotopologs of the hydroxymethyl radical. Because absorption to 3s is structureless, whereas absorption to $3p_x$ exhibits broad vibronic bands above the structureless 3s background, it is possible to distinguish between dissociation via 3s and $3p_x$.[20−22] Below we discuss dissociation mechanisms leading to channels I−III and associate them with the relevant conical intersections.[25,35]

A. Formaldehyde Channel. The images of H photofragments obtained at excitation energies where the C−H bond cannot be broken show that most of the formaldehyde products are generated with high KEs and possess excitation in the CO stretch and the $CH(D)_2$ deforomation modes (see Figures 2 and 3). The best fits to the KEDs generated in dissociation of CH_2OH and CH_2OD are obtained by using combination bands of the CO stretch and the ν_3 mode (CH_2 scissors; 1500 cm^{-1}). Fits using combination bands of CH_2 wag or rock with CO stretch give somewhat less satisfactory results but cannot be excluded. Although the fits are very good, the relative populations of the levels are difficult to determine accurately because of the proximity of some of the energy levels. However, the semiquantitative conclusion is robust: the main contributors to vibrational excitation in formaldehyde fragment are the CO stretch and the $CH(D)_2$ deformation modes (fundamentals, overtones, and combination bands). Rotational excitation is modest, and most of the available energy is released as kinetic energy.

This conclusion also makes physical sense. CO excitation is reasonable because of the large difference in C−O internuclear distance between $CH_2OH(D)$ and CH_2O.[48] It is also likely that, when the H atom of the dissociating O−H pushes against formaldehyde on the repulsive part of the PES, a symmetric nuclear motion such as CH_2 scissors will be excited. The observation of excitation in the CO stretch is in accordance with Yarkony's prediction of a conical intersection along the +*g* vector direction that propels the dissociating radical toward the repulsive part of the ground state PES and induces CO stretch excitation.[35] The pattern of fragment vibrational excitation does not change qualitatively at higher excitation energies in the 3s state, as seen in Figure 3, except that the extent of vibrational excitation increases somewhat with increasing photolysis energy. The recoil anisotropy parameter at high KEs (β = −0.7) is close to the maximum of −1.0 for a perpendicular transition and fast dissociation, as was found before.[20−22]

Referring again to Yarkony's calculations,[35] the small fraction of the formaldehyde fragments with a more statistical internal state distribution is predicted to arise from dissociation events along the −*g* direction, in which the gradients push the dissociating O−H in the direction of the bound region of the PES. Indeed, this is confirmed in our experiments, which demonstrate the generation of fragments with high internal energies and unresolved rovibrational state distributions (Figure 2). Similar bimodal energy distributions, consisting of a major high KE component with distinct structures and a minor, unstructured, lower KE component, are observed in all the investigated isotopologs (CH_2OH, CH_2OD, and CD_2OD). The absence of distinct structures in the low-KE part is consistent with a more statistical-like internal energy distribution in the formaldehyde fragment, in which rotational excitation is higher and all the allowed vibrational levels are populated. The similar distributions obtained for O−H and O−D bond breaking processes in $CH_2OH(D)$ indicate that the slow components are not due to tunneling (as observed, for example, in the dissociation of phenols and para-substituted phenols).[49,50] The hydrogen fragments with low KEs have nearly isotropic angular distributions, with β ranging from 0 to −0.4. These near-zero values of the β parameters do not imply here slow dissociation. Rather, out of plane motions can also reduce the anisotropy, especially when the fragments have such a broad distribution of internal energies.

B. Hydroxymethylene Channels. The two main questions regarding the *cis*- and *trans*-hydroxymethylene channels are (1) what are the mechanisms for their formation and (2) what are the relative populations of the cis- and trans-isomers? Yarkonly has predicted that formation of the higher lying *cis*-hydroxymethylene would be favored following a 3s/ground state conical intersection at large C−H internuclear distances and that this intersection would be accessible only above a small barrier above the dissociation threshold to this channel.[35] The calculations, which do not take zero-point energy into account, set this barrier at 2625 cm^{-1} above the channel II threshold. The energy separation of CH_2O and *trans*-HCOH has been calculated to be 18 126 cm^{-1} by Schreiner and coworkers,[48] whereas the cis−trans separation in hydroxymethylene was calculated to be 1536[48] and 1616[46,47] cm^{-1}.

The best determination of the energy thresholds for channels II and III are obtained from images recorded following $3p_x$ excitation, where the HCOH(D) yield is about 0.3 of CH_2O and both signals are much larger than the background. From the KEDs, we determine the energy difference between CH_2O and *trans*-HCOH at 18 084 ± 180 cm^{-1}, in excellent agreement with the calculated value.[48] The corresponding values returned by the fits for CHOD and CDOD are listed Table 3. The energy threshold for channel II is best determined from images where we zoom on the low KE regions to enhance resolution (Figure 6). In CH_2OH, the small amount of *trans*-HCOH that appears near the energy threshold for its formation is well

dx.doi.org/10.1021/jp404552g | J. Phys. Chem. A XXXX, XXX, XXX−XXX

separated in KE from the lowest KEs correlated with H_2CO. As the excitation energy increases, the maximum allowed KE correlated with HCOH becomes larger than the minimum KE of the H_2CO fragment and the two components coalesce. However, as shown in Figure 5, by using CH_2OD, these two components are distinguished.

With 3s excitation, the HCOD yield increases gradually (see Figures 3 and 4) near the channel II threshold. Because the H-fragment KEDs display no structural features we cannot determine whether *cis*-HCOH(D) appears at its threshold. It is likely that, as proposed by Yarkony, *trans*- and *cis*-HCOH(D) are first formed as minor products near their thresholds in dissociation events that sample the minimum region of the ground state PES and generate formaldehyde as the major fragment. This mechanism is consistent with the broad rovibrational excitations in the fragments. In our experiments, we cannot determine whether the 3s/ground state conical intersection at large C−H internuclear distances identified by Yarkony is accessible from the 3s state. We must wait for dynamical calculations to clarify this issue, though it is plausible that this tilted-cone conical intersection, while allowed energetically, is less efficient than the one along the O−H coordinate that leads mainly to channel I.[25,35]

In excitation to $3p_x$, for all the studied isotopologs we obtain better fits at all energies when assuming that the second peak in the KED associated with HCOH(D) is the ground state of the cis-isomer than ν_3 of *trans*-HCOH(D) or any other of its vibrational levels. Taking into account Yarkony's prediction that the main product following the conical intersections at large C−H distances is the cis-isomer,[25,35] we propose that the second peak in the KEDs correlated with hydroxymethylene is the ground vibrational state of the cis-isomer. In this case, the third peak can be assigned to ν_4 (CO stretch; ∼1300 cm^{-1}) of the cis-isomer. Results obtained with CD_2OD confirm and strengthen this interpretation. The H and D KEDs also allow us to determine experimentally the cis−trans separation in hydroxymethylene (HCOH, HCOD, and DCOD). The value for HCOH (Table 3) is in good agreement with the calculated one.[46−48]

V. SUMMARY AND CONCLUSIONS

The studies described above, together with previous experimental and theoretical work,[20−22,25,35] allow us to propose the following mechanisms for formaldehyde and hydroxymethylene formation in the photodissociation of hydroxymethyl radicals excited to the 3s and $3p_x$ states. The internal energy distribution in the formaldehyde fragment is bimodal. Most of the products are generated via a conical intersection between the 3s state and the ground state along the O−H bond coordinate that reaches the repulsive part of the ground state PES.[20−22,25,35] In agreement with Yarkony's predictions, the formaldehyde products have mostly high KEs and little rotational excitation but possess vibrational excitation in the CO-stretch and the CH(D) deformation modes, with best fits obtained with the scissors mode ν_3. A small fraction is produced with lower KEs and higher internal energies, again in agreement with Yarkony's suggestion that some of the dissociating radicals sample the minimum region of the PES before dissociating, giving rise to a broad range of internal energies in the formaldehyde product.

Near their thresholds, *trans*- and *cis*-HCOH (and their isotopologs) are probably generated by predissociation on the ground state PES following the 3s/ground state conical intersection along the O−H coordinate in a process that provides access to the minimum region on the ground state PES. The yield of hydroxymethylene via this pathway is small relative to the formaldehyde product, and it increases only slowly with excitation energy to the 3s state. The rovibrational energy distributions in HCOH(D) are broad, and no sharp threshold can be discerned at the cis-isomer threshold. It is likely that the 3s/ground state conical intersection seam along the C−H coordinate, which leads to direct C−H bond breaking via a tilted cone, is accessed less efficiently than the corresponding one along O−H, which is associated with a vertical cone and leads mainly to formaldehyde formation.

The situation changes abruptly when the $3p_x$ band origin is reached. The rotational excitation in the HCOH(D) fragments decreases and vibrational bands become discernible. The highest KE in the KEDs correlated with HCOH(D) corresponds to the ground vibrational level of the trans-isomer, and we find that its relative population decreases with increasing excitation energy. The next and most prominent peak in the KEDs is fit well as the ground vibrational level of the cis-isomer. *cis*-HCOH(D) is the most populated isomer, and other peaks in the KED can be modeled with its vibrational levels. This result agrees with the calculations of Hoffman and Yarkony who found a conical intersection seam between $3p_x$ and 3s (titled cone), which can then access both the O−H and C−H intersection seams between 3s and the ground state.[25] It is possible that starting from $3p_x$ gradients near the intersection seams propel CH_2OH efficiently toward routes that lead to the formation of both formaldehyde and *cis*-hydroxymethylene products along the O−H and C−H bond breaking coordinates, respectively. We note in closing that this is the first time that the cis-isomer of hydroxymethylene has been identified experimentally as a reaction product.

The results reported here, along with additional work in progress on energy distributions following excitation to the $3p_z$ state of the hydroxymethyl radical, have created a large set of benchmark data that can be compared now with theoretical calculations that include conical intersection seams and the dynamical evolution of the dissociating radicals through them. We hope that the work reported herein would serve as motivation for renewed theoretical efforts.

■ ASSOCIATED CONTENT

Supporting Information

Kinetic energy distributions and population analysis; additional fittings of selected KE distributions. This material is available free of charge via the Internet at http://pubs.acs.org.

■ AUTHOR INFORMATION

Corresponding Author

*(H.R.) E-mail: reisler@usc.edu.

Notes

The authors declare no competing financial interest.

■ ACKNOWLEDGMENTS

Support by the U.S. Department of Energy (DOE), Basic Energy Sciences, Grant No. DE-FG02-05ER15629, is gratefully acknowledged. We thank Dr. Amit Samanta for helpful discussions.

REFERENCES

(1) Lin, J. J.; Harich, S.; Lee, Y. T.; Yang, X. Dynamics of the $O(^1D)$ + CH_4 Reaction: Atomic Hydrogen Channel vs. Molecular Hydrogen Channel. *J. Chem. Phys.* **1999**, *110*, 10821.

(2) Lin, J. J.; Shu, J.; Lee, Y. T.; Yang, X. Multiple Dynamical Pathways in the $O(^1D)$ + CH_4 Reaction: A Comprehensive Crossed Beam Study. *J. Chem. Phys.* **2000**, *113*, 5287.

(3) Ahmed, M.; Peterka, D. S.; Suits, A. G. Imaging H Abstraction Dynamics in Crossed Molecular Beams: Cl + ROH Reactions. *Phys. Chem. Chem. Phys.* **2000**, *2*, 861−868.

(4) Rudic, S.; Murray, C.; Ascenzi, D.; Anderson, H.; Harvey, J. N.; Orr-Ewing, A. J. The Dynamics of Formation of HCl Products from the Reaction of Cl Atoms with Methanol, Ethanol, and Dimethyl Ether. *J. Chem. Phys.* **2002**, *117*, 5692−5706.

(5) Fockenberg, C.; Hall, G. E.; Preses, J.; Sears, T. J. Kinetics and Product Study of the Reaction of CH_3 Radicals with $O(^3P)$ Atoms Using Time Resolved Time-of-Flight Spectrometry. *J. Phys. Chem. A* **1999**, *103*, 5722−5731.

(6) Lindner, J.; Loomis, R. A.; Klaasen, J. J.; Leone, S. R. A Laser Photolysis/Time-Resolved Fourier Transform Infrared Emission Study of OH($X\ ^2\Pi$,v) Produced in the Reaction of Alkyl Radicals with $O(^3P)$. *J. Chem. Phys.* **1998**, *108*, 1944−1952.

(7) Seakins, P. W.; Leone, S. R. A Laser Flash Photolysis/Time-Resolved FTIR Emission Study of a New Channel in the Reaction of Methyl + Oxygen Atom: Production of Carbon Monoxide(v). *J. Phys. Chem.* **1992**, *96*, 4478−4485.

(8) Marcy, T. P.; Díaz, R. R.; Heard, D.; Leone, S. R.; Harding, L. B.; Klippenstein, S. J. Theoretical and Experimental Investigation of the Dynamics of the Production of CO from the CH_3 + O and CD_3 + O Reactions. *J. Phys. Chem. A* **2001**, *105*, 8361−8369.

(9) Bennett, C. J.; Chen, S. H.; Sun, B. J.; Chang, A. H. H.; Kaiser, R. I. Mechanistical Studies on the Irradiation of Methanol in Extraterrestrial Ices. *Astrophys. J.* **2007**, *1660*, 1588−1608.

(10) Bennett, C. J.; Kaiser, R. I. On the Formation of Glycolaldehyde ($HCOCH_2OH$) and Methyl Formate ($HCOOCH_3$) Interstellar Ice Analogs. *Astrophys. J.* **2007**, *66*, 899−909.

(11) Garrod, R. T.; Weaver, S. L. W.; Herbst, E. Complex Chemistry in Star-Forming Regions: An Expanded Gas-Grain Warm-Up Chemical Model. *Astrophys. J.* **2008**, *682*, 283−302.

(12) Laas, J. C.; Garrod, R. T.; Herbst, E.; Weaver, S. L. W. Contributions From Grain Surface and Gas Phase Chemistry to the Formation of Methyl Formate and Its Structural Isomers. *Astrophys. J.* **2011**, *728*, 71−79.

(13) Aristov, V.; Conroy, D.; Reisler, H. Symmetry and Lifetime of the Hydroxymethyl Radical in the 3p Rydberg State. *Chem. Phys. Lett.* **2000**, *318*, 393−401.

(14) Bauschlicher, J.; Charles, W.; Partridge, H. Heat of Formation of CH_2OH. *J. Phys. Chem.* **1994**, *98*, 1826−1829.

(15) Bruna, P. J.; Grein, F. Stability, Properties, and Electronic G Tensors of the H_2COH Radical. *J. Phys. Chem. A* **1998**, *102*, 3141−3150.

(16) Bruna, P. J.; Grein, F. The Electronic Spectrum of H_2COH Revisited. *J. Phys. Chem. A* **2001**, *105*, 8599−8603.

(17) Conroy, D.; Aristov, V.; Feng, L.; Reisler, H. Predissociation of the Hydroxymethyl Radical in the $3p_z$ Rydberg State: Formaldehyde + Hydrogen Atom Channel. *J. Phys. Chem. A* **2000**, *104*, 10288−10292.

(18) Curtiss, L. A.; Kock, L. D.; Pople, J. A. Energies of CH_2OH, CH_3O, and Related Compounds. *J. Chem. Phys.* **1991**, *95*, 4040−4043.

(19) Dóbé, S.; Bérces, T.; Turanyi, T.; Márta, F.; Grussdorf, J.; Temps, F.; Wagner, H. G. Direct Kinetic Studies of the Reactions Br + CH_3OH and CH_2OH + HBr: The Heat of Formation of CH_2OH. *J. Phys. Chem.* **1996**, *100*, 19864−19873.

(20) Feng, L.; Demyanenko, A. V.; Reisler, H. O−D Bond Dissociation from the 3s State of Deuterated Hydroxymethyl Radical (CH_2OD). *J. Chem. Phys.* **2003**, *118*, 9623−9628.

(21) Feng, L.; Demyanenko, A. V.; Reisler, H. Competitive C−H and O−D Bond Fission Channels in the UV Photodissociation of the Deuterated Hydroxymethyl Radical CH_2OD. *J. Chem. Phys.* **2004**, *120*, 6524−6530.

(22) Feng, L.; Huang, X.; Reisler, H. Photodissociative Spectroscopy of the Hydroxymethyl Radical (CH_2OH) in the 3s and $3p_x$ States. *J. Chem. Phys.* **2002**, *117*, 4820−4824.

(23) Feng, L.; Reisler, H. Photodissociation of the Hydroxymethyl Radical from the $2^2A''(3p_z)$ State: H_2CO and HCOH Products. *J. Phys. Chem. A* **2004**, *108*, 9847−9852.

(24) Feng, L.; Wei, J.; Reisler, H. Rotationally Resolved Infrared Spectroscopy of the Hydroxymethyl Radical (CH_2OH). *J. Phys. Chem. A* **2004**, *108*, 7903−7908.

(25) Hoffman, B. C.; Yarkony, D. R. Photodissociation of the Hydroxymethyl Radical. I. The Role of Conical Intersections in Line Broadening and Decomposition Pathways. *J. Chem. Phys.* **2002**, *116*, 8300−8306.

(26) Johnson, R. D., III; Hudgens, J. W. Structure and Thermochemical Properties of Hydroxymethyl (CH_2OH) Radicals and Cations Derived from Observations of the B(3p) ← X Electronic Spectra and from ab Initio Calculations. *J. Phys. Chem.* **1996**, *100*, 19874−19890 and references therein..

(27) Kamarchik, E.; Rodrigo, C.; Bowman, J. M.; Reisler, H.; Krylov, A. I. Overtone-Induced Dissociation and Isomerization Dynamics of the Hydroxymethyl Radical (CH_2OH and CD_2OH). I. A Theoretical Study. *J. Chem. Phys.* **2012**, *136*, 084304.

(28) Marenich, A. V.; Boggs, J. E. A Variational Study of Nuclear Dynamics and Structural Flexibility of the CH_2OH Radical. *J. Chem. Phys.* **2003**, *119*, 3098−3105.

(29) Marenich, A. V.; Boggs, J. E. Structural and Thermochemical Properties of the Hydroxymethyl (CH_2OH) Radical: A High Precision ab Initio Study. *J. Chem. Phys.* **2003**, *119*, 10105−10114.

(30) Oehlers, C.; Wagner, H. G.; Ziemer, H.; Temps, F.; Dóbé, S. An Investigation of the D/H Addition-Elimination and H Atom Abstraction Channels in the Reaction D + H_2CO in the Temperature Range 296 K ≤ T ≤ 780 K. *J. Phys. Chem. A* **2000**, *104*, 10500−10510.

(31) Pagsberg, P.; Munk, J.; Sillesen, A.; Anastasi, C. UV Spectrum and Kinetics of Hydroxymethyl Radicals. *Chem. Phys. Lett.* **1988**, *146*, 375−381.

(32) Ryazanov, M.; Rodrigo, C.; Reisler, H. Overtone-Induced Dissociation and Isomerization Dynamics of the Hydroxymethyl Radical (CH_2OH and CD_2OH). II. Velocity Map Imaging Studies. *J. Chem. Phys.* **2012**, *136*, 084305.

(33) Walch, S. P. Computed Barrier Heights for H + CH_2O ↔ CH_3O ↔ CH_2OH. *J. Chem. Phys.* **1993**, *98*, 3076−3077.

(34) Wei, J.; Karpichev, B.; Reisler, H. Unimolecular Processes in CH_2OH Below the Dissociation Barrier: O−H Stretch Overtone Excitation and Dissociation. *J. Chem. Phys.* **2006**, *125*, 34303−34310.

(35) Yarkony, D. R. Statistical and Nonstatistical Nonadiabatic Photodissociation from the First Excited State of the Hydroxymethyl Radical. *J. Chem. Phys.* **2005**, *122*, 084316.

(36) Jacox, M. E. The Reaction of Excited Argon Atoms and of F Atoms with Methanol. Vibrational Spectrum of CH_2OH Isolated in Solid Argon. *Chem. Phys.* **1981**, *59*, 213−230.

(37) Jacox, M. E.; Milligan, D. E. Matrix Isolation Study of the Vacuum-Ultraviolet Photolysis of Methanol. The Infrared Spectrum of the CH_2OH Free Radical. *J. Mol. Spectrosc.* **1973**, *47*, 148−162.

(38) Dulcey, C. S.; Hudgens, J. W. Multiphoton Ionization Spectroscopy and Vibrational Analysis of a 3p Rydberg State of the Hydroxymethyl Radical. *J. Chem. Phys.* **1986**, *84*, 5262−5270.

(39) Ryazanov, M.; Reisler, H. Improved Sliced Velocity Map Imaging Apparatus Optimized for H Photofragments. *J. Chem. Phys.* **2013**, *138*, 144201.

(40) Ryazanov, M. Development and Implementation of Methods for Sliced Velocity Map Imaging. Studies of Overtone-Induced Dissociation and Isomerization Dynamics of Hydroxymethyl Radical (CH_2OH and CD_2OH). Ph.D. Dissertation, University of Southern California, 2012.

(41) Blowers, P.; Masel, R. I. Calculated Vibrational Spectra for CH_nOH_m Species. *J. Phys. Chem. A* **2000**, *104*, 34−44.

(42) Shao, Y.; Fusti-Molnar, L.; Jung, Y.; Kussmann, J.; Ochsenfeld, C.; Brown, S. T.; Gilbert, A. T. B.; Slipchenko, L. V.; Levchenko, S. V.; O'Neill, D. P.; et al. Advances in Methods and Algorithms in a Modern

Quantum Chemistry Program Package. *Phys. Chem. Chem. Phys.* **2006**, *8*, 3172−3191.
(43) Western, C. M. *PGOPHER 2010*, a Program for Simulating Rotational Structure; University of Bristol: Bristol, U.K., 2010; see http://pgopher.chm.bris.ac.uk.
(44) Clouthier, D. J.; Ramsay, D. A. The Spectroscopy of Formaldehyde and Thioformaldehyde. *Annu. Rev. Phys. Chem.* **1983**, *34*, 31−58.
(45) Bouwens, R. J.; Hammerschmidt, J. A.; Grzeskowiak, M. M.; Stegink, T. A.; Yorba, P. M.; Polik, W. F. Pure Vibrational Spectroscopy of S_0 Formaldehyde by Dispersed Fluorescence. *J. Chem. Phys.* **1996**, *104*, 460−479.
(46) Koziol, L.; Mozhayskiy, V. A.; Braams, B. J.; Bowman, J. M.; Krylov, A. I. Ab Initio Calculation of the Photoelectron Spectra of the Hydroxycarbene Diradicals. *J. Phys. Chem. A* **2009**, *113*, 7802−7809.
(47) Koziol, L.; Wang, Y. M.; Braams, B. J.; Bowman, J. M.; Krylov, A. I. The Theoretical Prediction of Infrared Spectra Of *trans*- and *cis*-Hydroxycarbene Calculated Using Full Dimensional ab Initio Potential Energy and Dipole Moment Surfaces. *J. Chem. Phys.* **2008**, *128*, 4310.
(48) Schreiner, P. R.; Reisenauer, H. P.; Pickard, F. C.; Simmonett, A. C.; Allen, W. D.; Matyus, E.; Csaszar, A. G. Capture of Hydroxymethylene and Its Fast Disappearance Through Tunnelling. *Nature* **2008**, *453*, 906−909.
(49) Dixon, R. N.; Oliver, T. A. A.; Ashfold, M. N. R. Tunnelling Under a Conical Intersection: Application to the Product Vibrational State Distributions in the UV Photodissociation of Phenols. *J. Chem. Phys.* **2011**, *134*, 194303.
(50) Karsili, T. N. V.; Wenge, A. M.; Harris, S. J.; Murdock, D.; Harvey, J. N.; Dixon, R. N.; Ashfold, M. N. R. O−H Bond Fission in 4-Substituted Phenols: S_1 State Predissociation Viewed in a Hammett-Like Framework. *Chem. Sci.* **2013**, *4*, 2434−2446.